Morphology and phase diagram of complex block copolymers: *ABC* linear triblock copolymers

Ping Tang, Feng Qiu,* Hongdong Zhang, and Yuliang Yang

Department of Macromolecular Science, The Key Laboratory of Molecular Engineering of Polymers,
Ministry of Education, Fudan University, Shanghai 200433, China
(Received 22 October 2003; published 30 March 2004)

Using a real space implementation of the self-consistent field theory for the polymeric system, we explore microphases of *ABC* linear triblock copolymers. For the sake of numerical tractability, the calculation is carried out in a two-dimensional (2D) space. Seven microphases are found to be stable for the *ABC* triblock copolymer in 2D, which include lamellae, hexagonal lattice, core-shell hexagonal lattice, tetragonal lattice, lamellae with beads inside, lamellae with beads at the interface, and hexagonal phase with beads at the interface. By systematically varying the composition, triangle phase diagrams are constructed for four classes of typical triblock polymers in terms of the relative strengths of the interaction energies between different species. In general, when both volume fractions and interaction energies of the three species are comparable, lamellar phases are found to be the most stable. While one of the volume fractions is large, core-shell hexagonal or tetragonal phases can be formed, depending on which of the blocks dominates. Furthermore, more complex morphologies, such as lamellae with beads inside, lamellae with beads at the interface, and hexagonal phases with beads at the interface compete for stability with lamellae structures, as the interaction energies between distinct blocks become asymmetric. Our study provides guidance for the design of microstructures in complex block copolymers.

I. INTRODUCTION

The ability of block copolymers to self-assemble into a variety of fascinating periodic nanoscale morphologies has received much attention both experimentally and theoretically. The simplest and most typical block copolymers are linear *AB* diblock copolymers and their morphologies have been studied for decades. Four equilibrium phases for diblock copolymers, i.e., lamellae, complex gyroid, hexagonally packed cylinders, and body-centered-cubic spheres, have been found as the asymmetry in the composition of the blocks increases below the order-disorder transition temperature [1]. It is recognized both in experiment and theory that the ordered morphologies of *AB* diblock copolymers depend on three tunable molecular parameters: f_A, the composition (volume fraction) of block *A*, and χ_{AB}, the Flory-Huggins interaction parameter dependent on the temperature, representing interaction between the distinct *A* and *B* segments, and *N*, the total degree of polymerization of the diblock copolymer. However, as the number of distinct blocks is increased from two to three, say *ABC* triblock copolymers, both the complexity and variety of self-assembled structures are significantly increased. For triblock copolymers, the microphases not only depend on the composition and the interaction energies between distinct blocks, but also on particular molecular architectures. Therefore, distinctively new features absent in diblock copolymers arise in triblock copolymers. For instance, switching the sequence of an *AB* diblock copolymer to *BA* (diblock copolymer) does not change the equilibrium phase diagram, for an *ABC* triblock

copolymer, however, the microphase that can form significantly depends on the sequence of the blocks, i.e., whether it is sequenced *A-B-C*, *B-C-A* or *C-A-B*. In fact, recent experiments and theories have provided detailed evidence of the profound effects of block sequencing on their equilibrium morphologies [2-6].

Several theoretical approaches have been used to describe the microscopic morphologies for block copolymers. The Landau mean field theory by Leibler in weak-segregation limit [7], the analytical approaches by Helfand [8], Semenov [9] in strong-segregation limit, the density functional theory (DFT) of Ohta and Kawasaki [10], and recent Monte Carlo simulations for ABC star copolymers by Gemma *et al.* [11], have proven to capture essential features of the phase behavior of block copolymers. Among these theoretical methods, weak and strong-segregation theories and DFT are all mean-field theory with a number of additional approximations. These approximations, however, lead to large inaccuracies in determining the phase structure both for diblock and triblock copolymers [12,33]. Monte Carlo simulation methods, on the other hand, are computationally expensive. To date, the most accurate mean-field theory to investigate and screen the microphase structure is the self-consistent field theory (SCFT). The Fourier space implementation of the SCFT was proposed by Matsen and Schick [13], which allows the unification in weak and strong-segregation theories. This method is effective and precise, but need *a prior* assumption of the symmetry of the ordered structure, which makes it unsuitable for the discovery of previously unknown microphases in complex copolymers. To overcome this disadvantage, Drolet and Fredrickson have recently proposed a new combinatorial screening method [14,15,32], which involves a direct implementation of SCFT in real space in an adaptive arbitrary cell and proves very successful as applied to complex copolymer melts. A similar numerical methodology, which is based on

---

*Author to whom correspondence should be addressed; electronic address: fengqiu@fudan.edu.cn

DFT with some approximations in the strong-segregation regime and does not require the assumption of the microphase symmetry, was also used to explore the phase structure of various ABC triblock copolymer melts [18].

In the mean field level, five tunable parameters, i.e., the three interaction energies characterized by $\chi_{AB}N$, $\chi_{BC}N$, and $\chi_{AC}N$, respectively, and two independent compositions of components A and B, f_A and f_B ($f_C = 1 - f_A - f_B$) are required to specify a linear ABC triblock copolymer comprising three distinct blocks. Due to the large parameter space controlling the morphologies and the difficulties in numerical implementation, to date, theoretical investigation carried out in this area is quite limited and the phase behavior is less understood compared to the diblock counterpart [15-19]. Systematic investigations on how the phase behavior is related to the molecular characteristics are still desired. Furthermore, most of the studies, either in theory [19] or experiments [2,3,20,21] only covered limited parameter space of triblock copolymers, such as symmetric triblock copolymers. One exception is the three-component triangle phase diagram for triblock copolymers reported by Zheng and Wang [16], using an approximate DFT developed by Ohta and Kawasaki [10,22]. Unfortunately, the DFT they used was limited in the strong segregation regime and failed when the volume fraction of the middle block (f_B) is small. [16].

In this article, we use a combinatorial screening method based on the real space implementation of the SCFT, originally proposed by Drolet and Fredrickson [14,15], to search the equilibrium microphases of ABC linear triblock copolymer melts. Based on these microphases three-component triangle phase diagrams in the entire range of copolymer compositions are constructed. The influence of the compositions, interaction energies between distinct blocks and their relative strengths on the morphology is investigated systematically. Moreover, our method for ABC triblock copolymers recovers the proper diblock limit for small f_B.

II. THEORETICAL METHOD

We consider n linear ABC triblock copolymers each of polymerization N, with a volume V and compositions (average volume fractions) f_A and f_B ($f_C = 1 - f_A - f_B$) respectively. In the self-consistent mean-field theory, the many interacting chains are reduced to that of independent chains subject to an external (mean) field, created by the other chains. The fundamental quantity to be calculated in mean-field studies is the polymer segment probability distribution function, $q(\mathbf{r},s)$, representing the probability of finding segment s at position $\mathbf{r}$. It satisfies a modified diffusion equation using a flexible Gaussian chain model [23,24]:

$$\frac{\partial q(\mathbf{r},s)}{\partial s} = \frac{a^2}{6}\nabla^2 q(\mathbf{r},s) - [\gamma_A(s)\omega_A(\mathbf{r}) + \gamma_B(s)\omega_B(\mathbf{r})$$
$$+ \gamma_C(s)\omega_C(\mathbf{r})]q(\mathbf{r},s), \qquad (1)$$

where a is the Kuhn length of the polymer segment and $\omega_K(\mathbf{r})$ is the self-consistent field representing the interaction exerted to the species K, and $\gamma_K(s)$ is 1 if s belongs to blocks K and 0 otherwise. The initial condition is $q(\mathbf{r},0)$

$= 1$. Because the two ends of triblock chains are distinct, a second end-segment distribution function $q^+(\mathbf{r},s)$ is needed. It satisfies Eq. (1) only with the right-hand side multiplied by -1, and the initial condition, $q^+(\mathbf{r},N) = 1$. Accordingly the partition function of a single chain subject to the mean field $\omega_K(\mathbf{r})$, can be written as $Q = \int d\mathbf{r} q(\mathbf{r},s)q^+(\mathbf{r},s)$ in terms of $q(\mathbf{r},s)$ and $q^+(\mathbf{r},s)$. Note that Q is independent of the contour length parameter of the chain, s.

With the above description, the free energy of the system is given by

$$F/nk_BT = -\ln(Q/V) + (1/V)\int d\mathbf{r}[\chi_{AB}N\phi_A\phi_B$$
$$+ \chi_{BC}N\phi_B\phi_C + \chi_{AC}N\phi_A\phi_C - \omega_A\phi_A - \omega_B\phi_B$$
$$- \omega_C\phi_C - \xi(1 - \phi_A - \phi_B - \phi_C)], \qquad (2)$$

where ϕ_A, ϕ_B and ϕ_C are the monomer density field normalized by the local volume fractions of A, B and C, respectively. $\xi(\mathbf{r})$ is the potential field that ensures the incompressibility of the system, also known as a Lagrange multiplier. Minimizing the free energy in Eq. (2) with respect to ϕ_A, ϕ_B, ϕ_C, ω_A, ω_B, ω_C, and ξ leads to the following self-consistent field equations that describe the equilibrium morphology:

$$\omega_A(\mathbf{r}) = \chi_{AB}N\phi_B(\mathbf{r}) + \chi_{AC}N\phi_C(\mathbf{r}) + \xi(\mathbf{r}), \qquad (3)$$

$$\omega_B(\mathbf{r}) = \chi_{AB}N\phi_A(\mathbf{r}) + \chi_{BC}N\phi_C(\mathbf{r}) + \xi(\mathbf{r}), \qquad (4)$$

$$\omega_C(\mathbf{r}) = \chi_{AC}N\phi_A(\mathbf{r}) + \chi_{BC}N\phi_B(\mathbf{r}) + \xi(\mathbf{r}), \qquad (5)$$

$$\phi_A(\mathbf{r}) + \phi_B(\mathbf{r}) + \phi_C(\mathbf{r}) = 1, \qquad (6)$$

$$\phi_A(\mathbf{r}) = \frac{V}{NQ}\int_o^{f_AN} ds\, q(\mathbf{r},s)q^+(\mathbf{r},s), \qquad (7)$$

$$\phi_B(\mathbf{r}) = \frac{V}{NQ}\int_{f_AN}^{(f_A+f_B)N} ds\, q(\mathbf{r},s)q^+(\mathbf{r},s), \qquad (8)$$

$$\phi_C(\mathbf{r}) = \frac{V}{NQ}\int_{(f_A+f_B)N}^{N} ds\, q(\mathbf{r},s)q^+(\mathbf{r},s). \qquad (9)$$

The numerical implementation of the above self-consistent equations first proposed by Matsen and Schick has been successfully used to calculate the phase behavior of diblock copolymers [13]. However, this method requires *prior* assumed mesophase symmetry and thus the discovery of new complex morphologies is limited. Here we solve Eqs. (3)–(9) directly in real space by using a combinatorial screening algorithm proposed by Drolet and Fredrickson [14,15]. The algorithm consists of randomly generating the initial values of the fields $\omega_K(\mathbf{r})$. Using a Crank-Nicholson scheme and alternating-direct implicit (ADI) method [25], the diffusion equations are then integrated to obtain q and q^+, for $0 \le s \le 1N$. Next, the right-hand sides of Eqs. (7)–(9)

are evaluated to obtain new expression values for the volume fractions of blocks A, B, and C. $\xi(\mathbf{r})$ is then chosen to be

$$\xi(\mathbf{r}) = \lambda[1 - \phi_A(\mathbf{r}) - \phi_B(\mathbf{r}) - \phi_C(\mathbf{r})], \qquad (10)$$

where λ is large enough to enforce the incompressibility of the system, i.e., Eq. (6), and the resulting density profiles and free energies should be independent of its particular value. Finally, the potential fields $\omega_K(\mathbf{r})$ and $\xi(\mathbf{r})$ are updated using Eqs. (3)–(5) and (10) by means of a linear mixing of new and old solutions. These steps are repeated until the relative free energy changes at each iteration are reduced to 10^{-4}. It should be noted that the simulation box size has been found to influence the final morphologies [18]. Therefore each minimization of the free energy is iterated with respect to variety of reasonable sizes of the simulation cell to obtain the equilibrium structures. In order to avoid the real space method becoming trapped in a metastable state, random noises are added on the fields to disturb the morphology formed in the iterations. Furthermore, each minimization is run several times using different initial random guess of the potential fields $\omega_K(\mathbf{r})$ to ensure that the exact equilibrium morphology has been obtained. In this fashion, both typical ordered morphologies and the triangle phase diagram for triblock copolymers can be obtained by systematically changing the values of the parameters.

For the sake of numerical tractability, the implementation of the SCF equations is carried out in a two-dimensional $L_x \times L_y$ cell with periodic boundary conditions. The chain length of the polymers is fixed to be $N = 100$. The lattice spacings are chosen to be $dx = dy = a$, where a is the Kuhn length of the polymer segment. Since the radius of gyration of the polymer chain satisfies $R_g^2 = Na^2/6$ and typically the microstructure period $D \approx 2R_g$, the lattice spacings dx and dy are $\sim 0.1D$. The typical lattice sizes L_x and L_y are $\sim 10R_g$. Obviously, the results presented in this paper are subject to the 2D model, and hence may not obtain those intrinsic 3D structures, such as the cubic bcc and complex tricontinuous gyroid structures. However, the 2D model is not necessarily artificial. In fact, the potential applications of complex block copolymers as nanolithographic templates, membranes and precursors for quantum electronic arrays, often involve thin films with the thickness comparable to the radius of gyration of the block chains. Moreover, even in a 3D system, the microphases with translational invariance along certain directions, such as lamellar and cylindrical phases, can also be investigated by a 2D model.

III. RESULTS AND DISCUSSION

Figure 1 shows all 2D microphases discovered in this study for linear ABC triblock copolymers. The morphology is represented in the form of density plots with intensity proportional to the composition (volume fraction) of the triblock copolymers. Three different colors, blue, green and red are, respectively, assigned to A, B and C blocks. For a clear presentation of the final pattern, the linear dimensions of the unit cell are replicated 2 times in each direction.

For ABC linear triblock copolymers, three types of sequences can be formed, namely, A-B-C, B-C-A, and
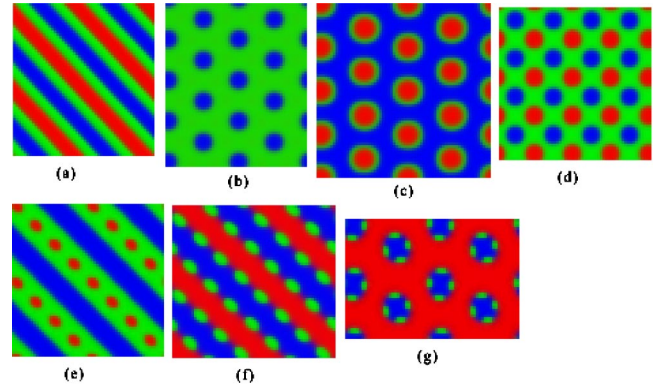

FIG. 1. (Color online) Schematic ordered morphologies for ABC linear block copolymers. (a) "Three-color" lamellar phase (LAM$_3$); (b) hexagonal lattice phase (HEX); (c) core-shell hexagonal lattice phase (CSH); (d) two interpenetrating tetragonal lattice phase (TET$_2$); (e) lamellar phase with beads inside (LAM +BD–I); (f) lamellar phase with beads at the interface (LAM +BD–II); (g) hexagonal phase with beads at the interface (HEX+BD).

C-A-B, respectively. If the binary interaction parameters χ_{AB}, χ_{BC} and χ_{AC} are different from each other, different sequences of blocks will lead to different phase behaviors for the system, even with the same composition parameters. In order to facilitate examining the influence of the sequences and relative strengths of the interaction energies, we define the ratios of the interactions as $R_1 = \chi_{AB}/\chi_{AC}$, $R_2 = \chi_{BC}/\chi_{AC}$, respectively. Then the system may be classified into four different classes in terms of relative strengths of the interaction energies: (1) $R_1 = R_2 = 1$, (2) $R_1 > 1$, $R_2 \geq 1$, (3) $R_1 < 1$, $R_2 \lesssim 1$, and (4) $R_1 < 1$, $R_2 > 1$.

A. Equal interaction energies ($R_1 = R_2 = 1$)

1. The influence of composition

We first discuss class (1), in which the interaction energies are equal between the three species. In this case the influence of copolymer compositions on the morphology is highlighted due to equal binary interactions between each block. The three-component triangle phase diagram covering the whole range of copolymer compositions is shown in Fig. 2. We concentrate our study on more experimentally interested intermediate-segregation regime because nonequilibrium effects are minimal, which will facilitate the comparison between the theory and experiment [26]. Therefore we have set $\chi_{AB}N = \chi_{BC}N = \chi_{AC}N = 35$ in Fig. 2, which is sufficient for the triblock copolymer to microphase separate. The increment of the volume fractions f_A, f_B and f_C in the phase diagram is 0.1. At each grid point, the equilibrium morphologies are obtained in the way described in Sec. II and represented by schematic symbols.

In the center region of the phase diagram in Fig. 2, where the volume fractions of the three components are comparable, "three color" lamellae (LAM$_3$) phases are formed, whose structure is shown in Fig. 1(a). At nearly equal volume fractions of the three species (symmetric triblock co-
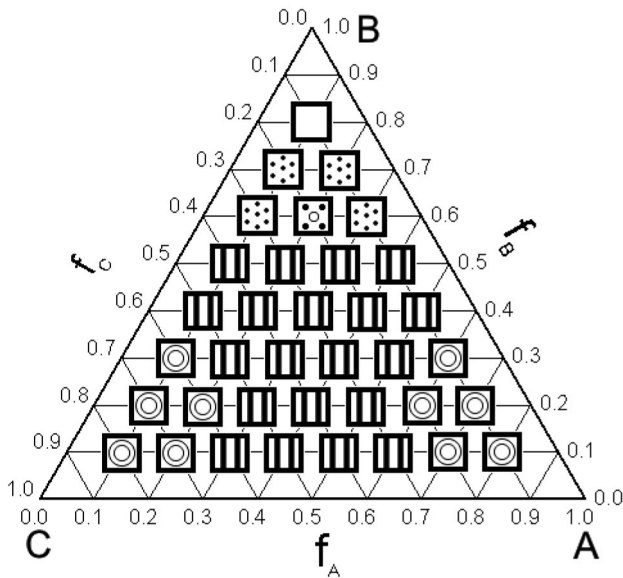
FIG. 2. Phase diagram for $\chi_{AB}N = \chi_{BC}N = \chi_{AC}N = 35$, i.e., $R_1 = R_2 = 1$. ▥ lamellae (LAM$_3$); ▨ two interpenetrating tetragonal lattice (TET$_2$); ◎ core-shell hexagonal lattice (CSH); ⊡ hexagonal lattice (HEX); ☐ disordered phase (DIS).

polymers, $f_A \approx f_B \approx f_C$), the LAM$_3$ phase with two characteristic lamellar widths are observed, i.e., $D_A \approx D_C \approx 2D_B$, where D_A, D_B, and D_C are widths of the A, B, and C lamellae, respectively. The same morphology was also predicted by Matsen using the Fourier space implementation of the SCFT [12] and by Zheng and Wang using the strong segregation theory [16]. Recently, the LAM$_3$ phase was observed in a poly(styrene-*b*-isoprene-*b*-ethylene oxide) melt [5]. We note that when one of the volume fractions, either f_A, or f_B, or f_C approaches zero, the copolymer reduces to a diblock copolymer and thus microphase separates into "two-color" lamellae (LAM$_2$) morphology. For middle block copolymers B forming the minority species ($f_B \lesssim 0.1$, for example), most of them are enriched at the interfaces between the two majority components (A and C blocks). On the contrary, for f_A or $f_C \lesssim 0.1$, the minority components A or C dissolve in the lamellae of the middle block B in the B/C or B/A lamellae at this χN.

Meanwhile, hexagonally packed lattice (HEX) phases are found at the corner B of the triangle phase diagram, where the middle block B dominates. In these microphases, the majority species of the middle block form the matrix, while the two minority components are mixed together to form the hexagonal lattice [Fig. 1(b)]. This morphology, however, have been reported not to arrange hexagonally but rather on a square lattice in the limit of strong segregation [16,19]. Near corners A and C, the morphology of core-shell hexagonal (CSH) phase occurs [Fig. 1 (c)], which is in agreement with the experimental findings [4,27]. In the CSH phase, the majority species A, which is one of the end blocks, forms the matrix, while the minority species, the C block, forms inner cores, and the middle block B forms the shells around the cores. A similar CSH phase with C block forming the matrix

and A forming the cores is also obtained near the C corner of the phase diagram. Near the B corner, where blocks B are the majority species, however, the stable phases have no internal A/C interfaces, the system forms two interpenetrating tetragonal lattice (TET$_2$) in a very limited region, as shown in Fig. 1(d).

In those regions near the edges of the triangle phase diagram in Fig. 2, where at least one of the volume fractions of the three blocks is very small, the three edges become phase diagrams for A-B ($f_C \rightarrow 0$), A-C ($f_B \rightarrow 0$) and B-C ($f_A \rightarrow 0$) diblock copolymers, respectively. Compared to the true diblock copolymers, in which the two ends are not constrained, however, for ABC triblock copolymers, the two ends of the middle block B are connected with either end of the blocks A or C. Therefore, the phase behavior cannot be expected to be exactly as those in diblock copolymers when one of the volume fractions is vanishing, but only when $f_B \rightarrow 0$, the ABC triblock copolymers would reproduce the phase behavior of diblock copolymers, which is a limit not properly treated by strong-segregation theories [16]. In Fig. 2, near the AC edge, the sequence of ordered morphologies follows: core-shell hexagonal→lamellar phases as the composition of one of the end blocks increases. The phase diagram in Fig. 2 clearly shows a reflection symmetry with respect to the vertical line where $f_A = f_C$ and thus switching the sequences of the outer blocks A and C ($ABC \rightarrow CBA$) does not alter the phase symmetry obtained. However, this rule will break when the binary interactions between the species become asymmetry ($\chi_{AB} \neq \chi_{BC}$), and will be discussed later.

For symmetric triblock copolymers, where $f_A = f_C$, as the volume fraction f_B increases, the ordered microphases change from LAM$_3$ to TET$_2$ and finally to HEX phases, as shown in Figs. 1(a), 1(d), and 1(b), respectively. This is a typical route investigated in experiments [2,3,21] and theories [15,19]. The TET$_2$ phase consists of two interpenetrating tetragonal lattices of A- and C-rich cylinders embedded in a matrix of B. It is noted that as f_B increases, the TET$_2$ phase competes for stability between the LAM$_3$ and HEX morphologies. There are also experimental [2,21,28] and theoretical [19] results showing a similar phase, composed of A and C cylinders tetragonal arranged within the B matrix. Apparently, the TET$_2$ phase is absent in AB diblock copolymers. These phenomena arise from the special characteristic of triblock copolymers. The A- and C-rich spheres must be placed close together because the B middle block copolymers have to bridge between them. As f_B further increases, the system chooses the HEX morphology because the hexagonal arrangement can fill the space very well. The balance of these two effects is responsible for choosing tetragonal or hexagonal lattice phase. The transitions from LAM$_3$ to TET$_2$ and from TET$_2$ to HEX occur at $f_B = 0.55$ and $f_B = 0.65$ (both with $f_A = f_C$), respectively. The region with TET$_2$ phases expands with the increase of the degree of segregation (increase of χN). We note that further increasing f_B result in a disordered melt without passing through a CsCl structure that was found in Ref. [16]. In fact, the CsCl phase is an
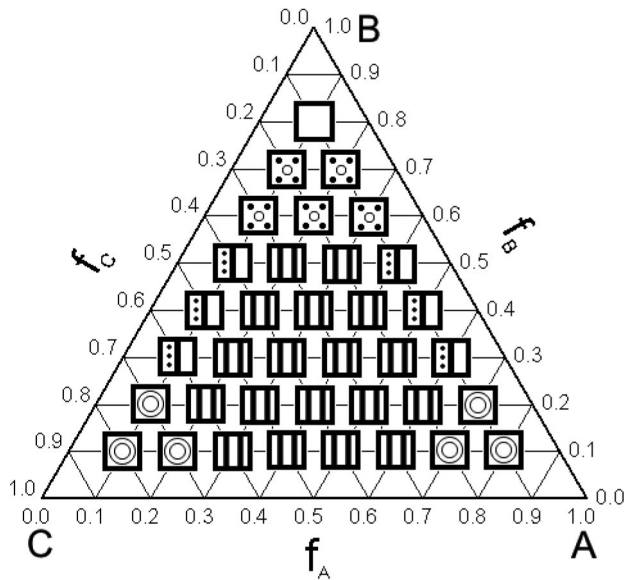
FIG. 3. Phase diagram for $\chi_{AB}N = \chi_{BC}N = \chi_{AC}N = 55$, i.e., $R_1 = R_2 = 1$. ▦ lamellae (LAM$_3$); ▨ two interpenetrating tetragonal lattice (TET$_2$); ◎ core-shell hexagonal lattice (CSH); ▥ lamellae with beads inside (LAM+BD−I); □ disordered phase (DIS).

FIG. 4. Phase diagram for $\chi_{AB}N = 78$, $\chi_{BC}N = 76$, $\chi_{AC}N = 20$, i.e., $R_1 = 3.9$, $R_2 = 3.8$. ▦ lamellae (LAM$_3$); ▤ lamellae with beads at the interface (LAM+BD−II); ⊡ hexagonal phase with beads at the interface (HEX+BD); ▨ hexagonal lattice (HEX); □ disordered phase (DIS).

intrinsic 3D structure and is not able to be distinguished from the TET$_2$ structure in the present 2D treatment.

2. Effects of the degree of segregation (the magnitude of χN)

As Matsen has pointed out, values of χN tend to affect the degree of segregation [12]. With increasing segregation, the local concentration (volume fraction) of the majority species in each domain reaches larger values and domain spacing increases while the interfacial width decreases. Therefore, in the weak and intermediate-segregation regions, different values of interaction energies χN become significant in determining the morphology of ABC triblock copolymers, just as that in diblock copolymers [7,29]. To illustrate the influence of χN on the morphology, the triangle phase diagram with a higher degree of segregation is shown in Fig. 3 where $\chi_{AB}N = \chi_{BC}N = \chi_{AC}N = 55$. Compared to Fig. 2, well-separated LAM$_3$ phases have now been observed. The reason is that the segregation is strong enough so the previously (at a lower χN value) mixed phase regions now start to phase separate to form three distinct phases. Furthermore, the stability region of the TET$_2$ phase is greatly enlarged. For $f_A = f_C$, the transition from LAM$_3$ to TET$_2$ occurs at $f_B = 0.55$ in Fig. 3, which is the same as that in Fig. 2.

Near the AB (BC) edge of the triangle diagram in Fig. 3, where the volume fraction of one of the end blocks f_C (f_A) is no more than 0.1, when $0.25 \lesssim f_B \lesssim 0.55$, a lamella-bead (LAM+BD−I) phase occurs to compete for stability with lamellar phases. As shown in Fig. 1(e), the LAM+BD−I phase is composed of C (A) beads regularly lined inside the B lamellae of the A/B (B/C) lamellae phase. Reducing unfavorable contacts is the main driving force to form this structure. It is obvious that this morphology, which is absent in Fig. 2 with lower χN, is enhanced with increasing the
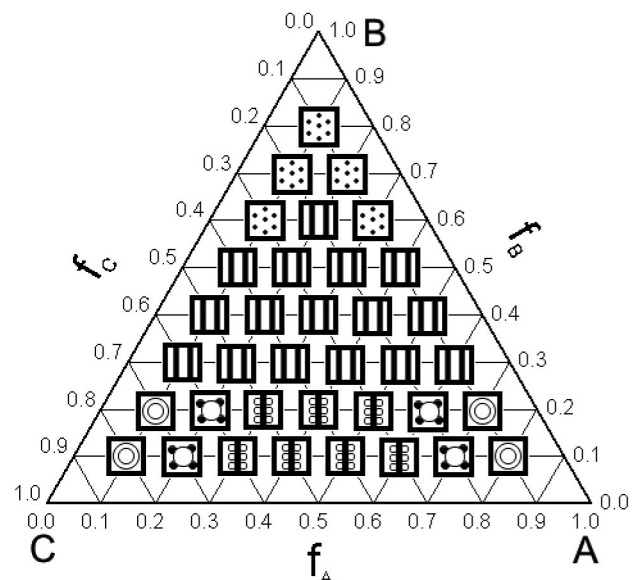
degree of segregation χN. A similar morphology has been observed by Zheng and Wang [16] in a theoretical treatment for ABC triblock copolymers using an approximate DFT method in the strong-segregation limit, rather than SCFT, and the region for this morphology appears at a smaller volume fraction ($f_C < 0.1$ or $f_A < 0.1$).

B. Nonequal interaction energies

In this section we discuss the three classes of ABC triblock copolymers with nonequal interaction energies between the three species to focus on the influence of the asymmetry of the interaction energy and the sequence of three blocks on the phase behavior.

Class (2): $R_1 > 1$, $R_2 \geqslant 1$. In this case, interactions between the end and middle blocks (A-B and B-C) are more unfavorable than that between the two end blocks (A-C). Therefore, the A/C interfaces are possible to be formed although there are no A-C chemical junctions. Figure 4 shows the phase diagram for $\chi_{AB}N = 78$, $\chi_{BC}N = 76$, $\chi_{AC}N = 20$, and thus $R_1 = 3.9$, $R_2 = 3.8$. In Fig. 4, near the edge of AC (where f_B is relatively small), the system tends to form morphologies such as A and C lamellae with circular beads of minority B blocks located at the A/C interfaces (LAM+BD−II) or hexagonal lattice with B beads at the interfaces (HEX+BD), whose structures are schematically shown in Figs. 1(f) and 1(g), respectively. It is interesting to compare these two predicted stable phases with the experimental findings by Stadler *et al.* [30], who studied poly(styrene-b-butadiene-b-methyl methacrylate) (PS-PB-PMMA), in which PS and PMMA are weakly incompatible while they both show a pronounced incompatibility toward PB. It was found that the PB midblock (7 and 12 wt. %) forms helical

strands surrounding the PS cylinders (25 and 26 wt. %) that are imbedded in the PMMA matrix, which is an intrinsic 3D structure. However, if the ultrathin section was along the main axis of the PS cylinders, a structure similar to LAM $+$ BD$-$II was observed; while if the section was perpendicular to the PS cylinders, HEX$+$BD phase was obtained. Since the two sections are all stable phases in 2D, it is reasonable to speculate that the helical structure is indeed a stable phase in 3D.

Furthermore, in Fig. 4, near corners A and C, when f_B $=0.1$, or $f_B=0.2$, the HEX$+$BD phase competes for stability with the core-shell morphology (CSH), due to more favorable contacts between the blocks A and C, as compared to strong incompatibility between the AB and BC contacts. The transition from HEX$+$BD to CSH structures was also observed in experiments for the system of PS-PB-PMMA with very short PB blocks by Krappe *et al.* [30,31]. Similar to our calculations, this morphology results from the relatively weak incompatibility between the two end blocks PS and PMMA.

It should be pointed out that in the case of equal interaction energies in Fig. 3, however, the middle B blocks always form layers in between the A and C domains (either LAM$_3$ or CSH structures). We also note that although the morphology of the LAM$+$BD$-$II [Fig. 1(f)] phase has an appearance similar to that of LAM$+$BD$-$I [Fig. 1(e)] previously observed in Fig. 3, they are different structures. In the former phase, the circular beads are formed by the middle blocks and thus are located at the interfaces of the lamellae comprising the end blocks, while in the latter phase, the beads are constructed by one of the end blocks A (C) and thereby are embedded in the B lamellae of the B/C (B/A) lamellae stacking.

In general, for these morphologies, the formation of the interface between A and C blocks is possible, due to the less incompatibility between the blocks A and C. Therefore, the region for LAM$+$BD$-$II phase expands with the decrease of $\chi_{AC}N$ and such effects will become even significant at stronger degree of segregation.

Another characteristic feature resulting from the weak incompatibility between the A and C block copolymers is that the morphology changes from TET$_2$ to HEX near corner B, where blocks B form the matrix. In this case, one of the relatively short end blocks A (C) can mix with another end block C (A) due to less unfavorable interaction between the A and C blocks and thus form cores embedded in the matrix of middle block B, to minimize the interfacial energies between the middle and end blocks.

Class (3): $R_1<1$, $R_2\lesssim1$. In this case, the interaction energy between the two end blocks A and C is more unfavorable than that of AB and BC contacts. The morphology that can avoid the A/C interface is favored and thus the region of the CSH phases expands. Figure 5 presents the phase diagram for $\chi_{AB}N=20$, $\chi_{BC}N=76$, and $\chi_{AC}N=78$, i.e., R_1 $=0.3$, $R_2=1.0$. Near the AB edge, where $f_C<0.35$, f_A >0.3, CSH structures are formed, with the C block forming the cores, the middle B blocks forming the shells, and the A blocks being the matrix, in order to achieve a lower interfa-
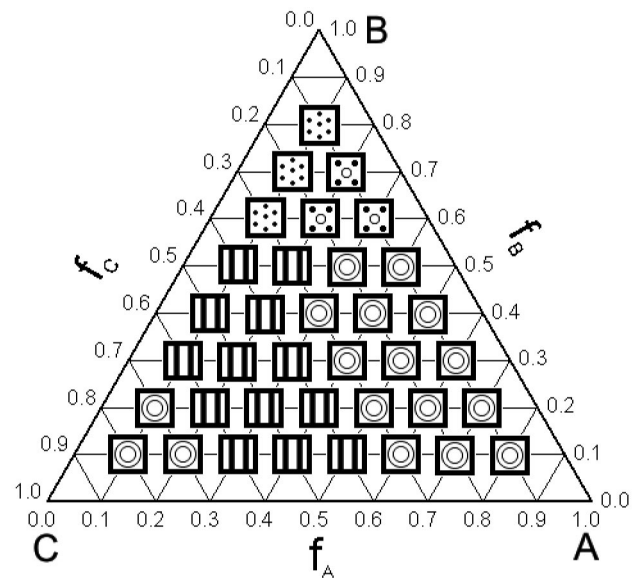

FIG. 5. Phase diagram for $\chi_{AB}N=20$, $\chi_{BC}N=76$, $\chi_{AC}N=78$, i.e., $R_1=0.3$, $R_2=1.0$. ▦ lamellae (LAM$_3$); ▨ two interpenetrating tetragonal lattice (TET$_2$); ◎ core-shell hexagonal lattice (CSH); ▦ hexagonal lattice (HEX).

cial energy. The relatively weaker incompatibility between the A and B blocks is responsible for the formation of the CSH phase. Obviously, the region of this core-shell type morphology will expand with reducing R_1. It is interesting to note that with similar ratios of the interaction energies, a coaxial cylinder phase was found by an analytical treatment in the strong-segregation limit [16], which is just the 3D version of the CSH structure.

Comparing Fig. 5 with Fig. 4, the phase diagram in Fig. 5 is obtained by simply changing the block sequence of the triblock copolymer in Fig. 4, i.e., from A-B-C to A-C-B. The different phase behavior observed in Fig. 4 and Fig. 5 illustrates the effect of the block sequencing in linear triblock copolymers. In particular, when the volume fractions of three components are comparable, lamellae phase is found in Fig. 4 in contrast to core-shell structure in Fig. 5. We note that in the strong-segregation limit the same effect has also been examined by Zheng and Wang [16]. Experimentally, a lamellar phase in 1:1:1 poly(isoprene-*b*-styrene-*b*-2-vinylpyridine) (ISP) has been observed by Mogi *et al.* [2,3,20], while a coaxial cylinder phase was found in SIP by Gido *et al.* [4], which shows the crucial dependence of the phase behavior of triblock copolymers on the sequencing of their blocks. Our calculation based upon SCFT confirms these experimental phenomena.

Class (4): $R_1<1$, $R_2>1$. In this case, the B and C blocks are more incompatible than A and B blocks. The system thus prefers the morphology that increases interfacial contacts between the A and B blocks as well as reduces the unfavorable contacts between the B and C species to balance the increase in the stretching energies. Figure 6 presents the phase diagram for $\chi_{AB}N=25$, $\chi_{BC}N=80$, and $\chi_{AC}N=60$, i.e., R_1 $=0.4$, $R_2=1.3$. When blocks B are the majority species ($f_B=0.5$, $0.2\lesssim f_A\lesssim0.4$), LAM$+BD-$I phase occurs due to
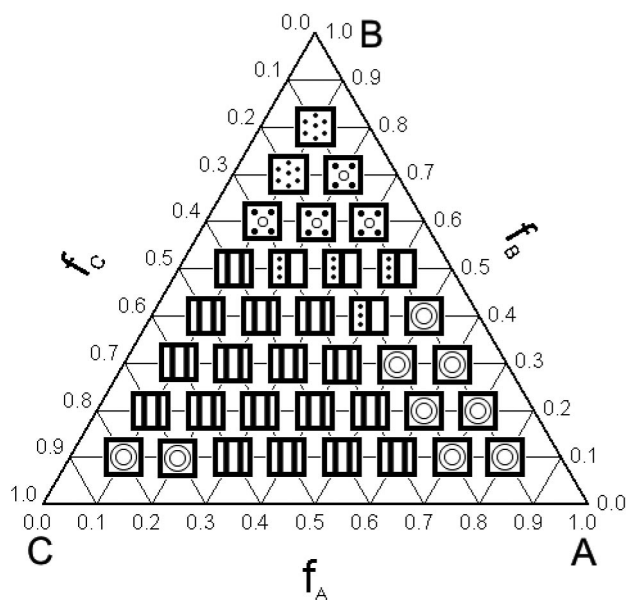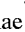
FIG. 6. Phase diagram for $\chi_{AB}N = 25$, $\chi_{BC}N = 80$, $\chi_{AC}N = 60$, i.e., $R_1 = 0.4$, $R_2 = 1.3$. ◎ core-shell hexagonal lattice (CSH); ▥ lamellae (LAM$_3$); ▤ lamellae with beads inside (LAM+BD−I); ▨ two interpenetrating tetragonal lattice (TET$_2$); ▦ hexagonal lattice (HEX).

the strong unfavorable contacts between blocks B and C. In contrast, in Fig. 3, LAM$_3$ phase is found in this region. Furthermore, CSH morphology near the AB edge of the phase diagram ($f_A \geq 0.5$) is observed and avoiding the interface between the A and C blocks is the main driving force for this phase.

IV. CONCLUSIONS

We have systematically searched the parameter space of the linear ABC triblock copolymers based on a real space implementation of SCFT. Seven different ordered morphologies in 2D are observed, including lamellae, hexagonal lattice, core-shell hexagonal lattice, tetragonal lattice, lamellae with beads inside, lamellae with beads located at interfaces, and hexagonal phase with beads at interfaces. By systematically varying the composition, triangle phase diagrams are constructed for four classes of typical triblock copolymers in terms of the relative strengths of the interaction energies between different species. The ordered morphologies of the ABC triblock copolymers not only depend on the composition, but also on the degree of segregation (values of χN) significantly. In general, when both the volume fractions and interaction energies of the three species are comparable, lamellar phases are found to be the most stable. While if one of the volume fractions is large, core-shell hexagonal or tetragonal phase can be formed, depending on which of the blocks dominates. Furthermore, more complex morphologies, such as lamellae with beads inside, lamellae with beads at the interface, and hexagonal phase with beads at the interface compete for stability with lamellae structures, as the interaction energies between distinct blocks become asymmetric. When the interaction energies between the three species are different to each other, the sequence of the blocks affects the phase behavior significantly. In particular, by switching the middle block and one of the end blocks, a change from lamellar phase to core-shell hexagonal phase is predicted for a typical class of ABC triblock copolymers, which is indeed the case for most of the experiments explored. The triangle phase diagrams we present may be guidance to designing the desired phase structures in terms of the composition of the ABC triblock copolymers, the values of interaction energies and their relative strengths.

[1] M. W. Matsen, J. Chem. Phys. **113**, 5539 (2000).

[2] Y. Mogi, H. Kotsuji, Y. Kaneko, K. Mori, Y. Matsushita, and I. Noda, Macromolecules **25**, 5408 (1992).

[3] Y. Mogi, K. Mori, Y. Matsushita, and I. Noda, Macromolecules **25**, 5412 (1992).

[4] S. P. Gido, D. W. Schwark, E. L. Thomas, and M. Goncalves, Macromolecules **26**, 2636 (1993).

[5] T. S. Bailey, C. M. Hardy III, T. H. Epps, and F. S. Bates, Macromolecules **35**, 7007 (2002).

[6] T. S. Bailey, H. D. Pham, and F. S. Bates, Macromolecules **34**, 6994 (2001).

[7] L. Leibler, Macromolecules **13**, 1602 (1980).

[8] E. Helfand and Z. R. Wasserman, Macromolecules **13**, 994 (1980).

[9] A. N. Semenov, Sov. Phys. JETP **61**, 733 (1985).

[10] T. Ohta and K. Kawasaki, Macromolecules **19**, 2621 (1986).

[11] T. Gemma, A. Hatano, and T. Dotera, Macromolecules **35**, 3225 (2002).

[12] M. W. Matsen, J. Chem. Phys. **108**, 785 (1998).

[13] M. W. Matsen and M. Schick, Phys. Rev. Lett. **72**, 2660 (1994).

[14] F. Drolet and G. H. Fredrickson, Phys. Rev. Lett. **83**, 4317 (1999).

[15] F. Drolet and G. H. Fredrickson, Macromolecules **34**, 5317 (2001).

[16] W. Zheng and Z.-G. Wang, Macromolecules **28**, 7215 (1995).

[17] C. Auschra and R. Stadler, Macromolecules **26**, 2171 (1993).

[18] Y. Bohot-Raviv and Z.-G. Wang, Phys. Rev. Lett. **85**, 3428 (2000).

[19] H. Nakazawa and T. Ohta, Macromolecules **26**, 5503 (1993).

[20] Y. Mogi, K. Mori, H. Kotsuji, Y. Matsushita, and I. Noda, Macromolecules **26**, 5169 (1993).

[21] Y. Mogi, M. Nomura, H. Kotsuji, K. Ohnishi, Y. Matsushita, and I. Noda, Macromolecules **27**, 6755 (1994).

[22] T. Ohta and K. Kawasaki, Macromolecules **23**, 2413 (1990).

[23] E. Helfand, J. Chem. Phys. **62**, 999 (1975).

[24] S. F. Edwards, Proc. Phys. Soc. London **85**, 613 (1965).

[25] W. H. Press, B. P. Flannery, S. A. Teukolsky, and W. T. Vetterling, *Numerical Recipes* (Cambridge University Press, Cambridge, England, 1989).

[26] P. M. Lipic, F. S. Bates, and M. W. Matsen, J. Polym. Sci., Part B: Polym. Phys. **37**, 2229 (1999).

[27] U. Breiner, U. Krappe, V. Abetz, and R. Stadler, Macromol. Chem. Phys. **198**, 1051 (1997).

[28] K. Jung, V. Abetz, and R. Stadler, Macromolecules **29**, 1076 (1996).

[29] S. Sakurai, T. Momii, K. Taie, M. Shibayama, S. Nomura, and T. Hashimoto, Macromolecules **26**, 485 (1993).

[30] U. Krappe, R. Stadler, and I. Voigt-Martin, Macromolecules **28**, 4558 (1995).

[31] C. Auschra and R. Stadler, Polym. Bull. (Berlin) **30**, 257 (1993).

[32] G. H. Fredrickson, V. Ganesan, and F. Drolet, Macromolecules **35**, 16 (2002).

[33] M. W. Matsen, J. Chem. Phys. **114**, 10 528 (2001).